

This is the accepted manuscript made available via CHORUS. The article has been published as:

## Evidence of high-spin Ru and universal magnetic anisotropy in $\text{SrRuO}_3$ thin films

A. J. Grutter, F. J. Wong, E. Arenholz, A. Vailionis, and Y. Suzuki

Phys. Rev. B **85**, 134429 — Published 17 April 2012

DOI: [10.1103/PhysRevB.85.134429](https://doi.org/10.1103/PhysRevB.85.134429)

# Evidence of High Spin Ru and Universal Magnetic Anisotropy in SrRuO<sub>3</sub> Thin Films

A. J. Grutter,<sup>1,2</sup> F. J. Wong,<sup>1</sup> E. Arenholz,<sup>3</sup> A. Vailionis,<sup>4,5</sup> and Y. Suzuki<sup>1,2</sup>

<sup>1</sup>*Department of Materials Science and Engineering,  
University of California, Berkeley, CA 94720, USA*

<sup>2</sup>*Materials Sciences Division, Lawrence Berkeley National Laboratory, Berkeley, CA 94720, USA*

<sup>3</sup>*Advanced Light Source, Lawrence Berkeley National Laboratory, Berkeley, CA 94720, USA*

<sup>4</sup>*Geballe Laboratory for Advanced Materials, Stanford University, Stanford, California, 94305, USA*

<sup>5</sup>*Stanford Institute for Materials and Energy Sciences,  
SLAC National Accelerator Laboratory, Menlo Park, California 94025, USA*

(Dated: March 21, 2012)

We have investigated the origins of enhanced saturated magnetic moment and strong strain dependent magnetic anisotropy in epitaxial films of the transition metal oxide SrRuO<sub>3</sub>. We find evidence for an enhancement of the carrier concentration and the stabilization of high-spin Ru<sup>4+</sup>. Through X-ray magnetic circular dichroism measurements, we also observe a strain dependent enhancement of the out-of-plane orbital magnetic moment. Such an enhancement is consistent with the universal out-of-plane anisotropy axis shown to occur in films in a variety of different crystallographic orientations. We explain all these effects in terms of an anisotropic reduction in the crystal field resulting from anisotropically reduced orbital overlap in distorted films.

PACS numbers:

## I. INTRODUCTION

Structural distortions give rise to modifications in electronic structure that can stabilize novel electronic and magnetic ground states. Transition metal complex oxides, with widely varying properties and strongly correlated electronic interactions, offer exciting model systems in which to study the stabilization of these new ground states via lattice distortions.<sup>1–3</sup> Recent advances in deposition techniques have allowed the development of atomically precise epitaxial complex oxide thin films. Thus, thin films of these materials are now being used to separate microstructural effects from those of interfaces and lattice distortions.

The ferromagnetic metal SrRuO<sub>3</sub> (SRO) is one such oxide that has attracted much attention. It is unique as the only known 4*d* transition metal oxide ferromagnet. In most 4*d* systems, the extended orbitals increase the bandwidth and decrease the density of states at the Fermi level, precluding Stoner-type ferromagnetism.<sup>4,5</sup> In SRO, however, strong hybridization of the Ru 4*d* and O 2*p* bands enhances the density of states at the Fermi level, resulting in ferromagnetic interactions and metallicity.<sup>6–8</sup> Consequently, bulk SRO exhibits strong magnetism for a 4*d* system, with a bulk Curie temperature (*T<sub>C</sub>*) of 160K and reported saturated moment values ranging from 1.1–1.6  $\mu_B$ /Ru<sup>4+</sup>.<sup>7,9–11</sup> Due to the large crystal field splitting, Ru<sup>4+</sup> ions are usually expected to be in a low spin state with an electron configuration of *t*<sub>2*g*</sub><sup>4</sup> (3↑, 1↓) corresponding to 2  $\mu_B$ /Ru<sup>4+</sup> ion — higher than what is experimentally observed. The lower experimental values of Ru moment in SRO have thus far been attributed to electron delocalization associated with itinerancy.<sup>7</sup> Until recently, there had been no report of a Ru based compound with a high spin state (4  $\mu_B$ /Ru<sup>4+</sup>) ion.

Thin films of SRO have been shown to exhibit highly

tunable, non bulk-like properties. Studies of SRO films have reported a metal-insulator transition, competition between ferromagnetic and antiferromagnetic states in ultrathin films, and spin-glass behavior.<sup>12–14</sup> Since we demonstrated that epitaxial strain could be used to enhance the saturation magnetization (*M<sub>S</sub>*) of SRO thin films, there have been several reports of similarly enhanced magnetic moment.<sup>15–18</sup> These experimental results, in which compressive strain enhanced the saturated moment, are at odds with theoretical studies where compressively strained (100) and (110) SRO films are predicted to have saturated magnetic moments suppressed from bulk values.<sup>19</sup> It is also predicted that an enhanced moment can be realized through the application of biaxial tension, although we are not aware of any experimental confirmation or contradiction of this prediction.<sup>19</sup>

Recent reports have also shown that when SRO thin films are grown on (100) and (110) SrTiO<sub>3</sub> (STO), they exhibit an out-of-plane easy axis which is independent of crystallographic orientation.<sup>14,18</sup> That is, when grown on (100) STO the film easy axis is in the [100] direction, but when grown on (110) STO the easy axis is in the [110] direction.<sup>14,18</sup> Additionally, the anisotropy is very strong, with different in-plane and out-of-plane moments reported at applied fields of up to 5T.<sup>14,18</sup>

In this paper, we demonstrate that both enhanced saturated magnetic moment and strong uniaxial anisotropy can be induced simultaneously through the application of compressive epitaxial strain. In (111) oriented films, the resulting distortions of the Ru octahedral environment may cause electrons to populate the newly split *e<sub>g</sub>* band, effectively placing the Ru in a high spin state and enhancing the magnetic moment. We find an increase in the carrier concentration consistent with the presence of such high spin Ru. SRO films grown under identical conditions on (100) and (110) substrates show simi-

lar behavior but are more consistent with a low spin Ru state. All films with enhanced saturated moment also show strong uniaxial magnetic anisotropy with an out-of-plane easy direction. By systematically varying the magnitude of the lattice distortions in the SRO samples, we conclusively show that these lattice distortions are the source of the enhanced Ru moment, larger carrier concentration, and strong magnetic anisotropy. We theorize that lattice distortions anisotropically alter the bonding in the Ru-O octahedra in a way that simultaneously reduces the quenching of the orbital moment and involves the  $e_g$  states in the magnetism, explaining all our observations.

## II. EXPERIMENT

One of the goals of this study is to understand the importance of the magnitude and symmetry of applied lattice distortions in stabilizing new magnetic ground states in thin films. To that end, SRO thin films were grown on (100) and (110)  $\text{SrTiO}_3$  (STO),  $(\text{LaAlO}_3)_{0.3}(\text{Sr}_2\text{AlTaO}_6)_{0.7}$  (LSAT) and  $\text{LaAlO}_3$  (LAO) as well as (111) STO in thicknesses ranging from 15 to 120 nm. This combination of substrates and thicknesses yielded tetragonally, monoclinically, and trigonally distorted films with film-substrate lattice mismatches that varied from -0.64% on STO and -1.8% on LSAT to -3.6% on LAO. Samples were grown using pulsed laser deposition in 60 mtorr  $\text{O}_2$  at a temperature of 700 °C and a laser fluence of approximately 1.3 J/cm<sup>2</sup>. They were then post-annealed in 100 torr  $\text{O}_2$  at 600 °C for 7 minutes.

SRO has an orthorhombic structure with bulk lattice parameters  $a = 5.57$  Å,  $b = 5.53$  Å,  $c = 7.84$  Å; however, it can be well represented as a pseudocubic perovskite with  $a = 3.93$  Å, which is the structure we will use to describe orientation throughout this paper.<sup>20–22</sup> Structural characterization was performed by X-ray diffraction in the form of  $\omega$  rocking curves,  $\theta$ - $2\theta$  scans, and reciprocal lattice maps taken on a Panalytical X'Pert Materials Research Diffractometer. Surface morphology was characterized by atomic force microscopy (AFM). Film thickness and stoichiometry were obtained by Rutherford backscattering spectrometry (RBS). Transport measurements were taken in a Quantum design PPMS system from 4–300 K in magnetic fields of up to 7 T. For magnetic characterization, we used a Quantum Design MPMS-5 SQUID magnetometer varying temperature and applied field. All saturated magnetization values were taken at a temperature of 10 K and an applied field of 5 T. X-ray absorption (XA) and X-ray magnetic circular dichroism (XMCD) spectra, taken at beamlines 4.0.2 and 6.3.1 of the Advanced Light Source at Lawrence Berkeley National Lab, were used to test for magnetic impurities such as Fe, Ni, or Co, to confirm elemental valence states, and to acquire element-specific magnetic information.

## III. STRUCTURE AND MORPHOLOGY

Such a systematic study of the effect of lattice distortions requires a set of consistently high quality samples and accurate characterization of the magnitude of the applied strain. To that end, we utilized a combination of structural and surface characterization techniques that indicate our SRO films are epitaxial, highly crystalline, stoichiometric, and smooth. Our  $\theta - 2\theta$  X-ray diffraction scans indicate high quality films with peaks corresponding exclusively to SRO and the substrates in the expected crystallographic orientations. Rocking curves of the film peaks showed excellent epitaxy with mosaic spreads as low as 0.038°. Among substrates of a particular orientation, mosaicity is inversely related to lattice mismatch, with films on STO showing smaller mosaic spread than films on LSAT and LAO, which show increasing mosaicity. Films on (100) and (110) STO have much lower mosaic spread than films on (111) STO.

A comparison of reciprocal lattice maps (RLMs) of SRO films grown on different substrates and in different orientations revealed a variety of strain states. By varying lattice mismatch from -0.7% to -3.8% and thickness from 15 to 120 nm we grew films that were coherently strained, partially relaxed, and fully relaxed. RLMs of the films grown on (100) and (110) STO show that films are strained up to thicknesses of 80 nm, but begin to show partial relaxation by 120 nm.<sup>15</sup> Films on LSAT begin to relax partially at thicknesses above 60 nm. On LAO, films are difficult to grow fully strained; 40–50 nm thick films are partially relaxed and full relaxation occurs by 80 nm.<sup>16</sup> These fully relaxed films on LAO, as well as the thicker partially relaxed films on STO, can serve as important reference samples. If lattice distortions are controlling the film properties, these films should show much more bulk-like behavior.

It is more difficult to stabilize coherently strained films in the (111) orientation. RLMs of the (321) reflection of films on (111) STO show greater relaxation than films of comparable thickness in other orientations. For SRO films on (111) STO, coherent strain can be maintained only for films less than 30 nm thick. This challenge is magnified in (111) oriented films on LSAT and LAO and we therefore only discuss films grown on (111) STO. In these films on (111) STO, we were able to obtain a variety of different strain states ranging from coherently strained to partially relaxed as film thickness was increased from 15 to 120 nm.

We found additional confirmation of film quality through characterization of surface morphology using AFM and film stoichiometry using RBS. AFM measurements reveal unit cell terraces on the smoothest films on (100) STO that transition to bunched steps for films grown on LSAT and rougher 3D islands on LAO where epitaxial strain is larger. Even these rougher films on LAO had roughnesses much lower than the film thickness. RBS measurements were consistent with  $\text{SrRuO}_3$ , showing a 1:1 ratio of Sr and Ru. It is much more diffi-

cult to accurately determine O content; all measurements are consistent to within experimental error with the expected stoichiometry. Thus, through a combination of AFM, X-ray diffraction, and RBS, we conclude that we have grown high-quality stoichiometric films of SRO in a wide variety of strain states.

#### IV. MAGNETISM

Having grown high quality SRO films in a variety of strain states, we examined the magnetic behavior of the films in order to correlate it with the structure. To examine the relationship between epitaxial strain, enhanced magnetic moment, and magnetic anisotropy, we used SQUID magnetometry to probe the saturated magnetic moment with the field applied in-plane and out-of-plane. We also used XMCD to determine the elemental origin of these effects and elucidate the ratio of spin and orbital contributions to the magnetic moment. We observed enhanced Ru magnetic moment in triclinically distorted (111) films relative to (100) and (110) SRO films, which are themselves enhanced relative to bulk SRO. This enhancement appears to be primarily due to an increase in the spin contribution to the magnetic moment, with a small increase in the orbital contribution as well. Additionally, the easy axes of all compressively strained films are out-of-plane regardless of substrate orientation. Both effects are strongly correlated to lattice distortions imposed by the substrate.

SQUID magnetometry revealed a strong dependence of the saturated moment on substrate orientation, as illustrated in Figure 1, which shows a typical series of films between 60-70nm thick on (100), (110), and (111) oriented STO. Compressively strained films of all orientations exhibited enhanced saturated magnetic moments compared to previous bulk and thin film values of 1.1-1.6  $\mu_B/\text{Ru}^{4+}$  regardless of film thickness. On all substrate materials, (110)-oriented films generally had higher saturated moments than (100) oriented films. However, all of our (100) and (110) films saturate at or below 2.35  $\mu_B/\text{Ru}^{4+}$  and can be explained in terms of a low spin moment of 2  $\mu_B/\text{Ru}^{4+}$  ions combined with a 10-15% orbital contribution (described later). Our completely relaxed films on (100) LAO showed much more bulk-like behavior, saturating at a magnetic moment of 1.2  $\mu_B/\text{Ru}^{4+}$ , while the thickest, partially relaxed films on (100) STO had saturated moments of 1.44  $\mu_B/\text{Ru}^{4+}$ . These observations indicate that our films are quite bulk-like in the absence of strain.

In contrast to (100) and (110) oriented films, SQUID magnetometry of SRO in the (111) orientation showed high saturated moments which suggest that trigonally distorted (111) SRO films are in a high spin Ru state characterized by a mix of  $t_{2g}$  and  $e_g$  states at the Fermi level. Numerous films on (111) STO exhibit values in excess of 2.4  $\mu_B/\text{Ru}^{4+}$ , with some as high as 3.5  $\mu_B/\text{Ru}^{4+}$ . Such large moments cannot be explained in terms of a

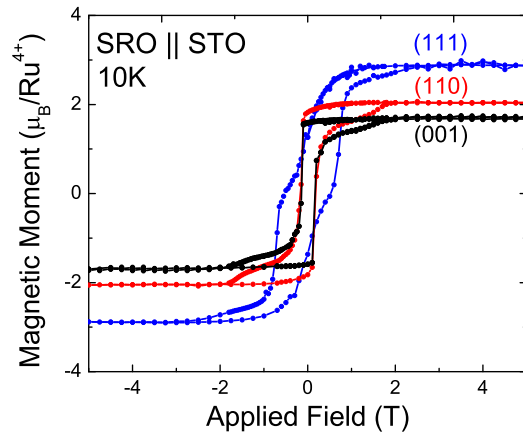


FIG. 1: (color online) Hysteresis loops taken at 10K of 60-70 nm thick films on (100), (110), and (111) oriented STO showing the strong relationship between strain orientation and saturated moment. It should be noted that the loop of the (111) oriented film displays a pinched shape characteristic of two magnetic states. This effect is consistent with the stabilization of a mixture of high and low-spin states

low spin Ru state. Thus, we can see that the symmetry of the applied lattice distortion, in addition to its magnitude, is crucial in determining the magnetic state.

Within a given orientation, we also observed significant variation between films of different thicknesses and between films on different substrate materials. By growing the (100) oriented films at varying thicknesses on STO, LSAT, and LAO, we synthesized (100) SRO films with a range of strain states and saturated Ru moments and attempted to correlate the two using RLMs. Although it is straightforward to extract a specific strain from the RLM in a coherently strained film, there is a distribution of film lattice parameters in partially relaxed films that makes it difficult to extract a specific value for strain. Thus, to quantify the lattice distortion, we use the mismatch between the average measured film lattice constant and the bulk lattice constant. The high single crystalline quality of the films, indicated by their low mosaic spread, makes this approximation well justified and the calculated strain represents well the degree of relaxation in the film. Figure 2(a) & (b) shows strain vs. saturated moment in (100) and (111) oriented SRO films respectively, along with typical reciprocal space maps showing relative amounts of relaxation. In these space maps, alignment of the film and substrate peaks along the in-plane axis indicates a coherently strained film while an offset in the film peak means that total or partial relaxation has occurred. We found that films with larger strains always had higher saturated magnetic moments. In (111) films, there was a rapid increase in magnetic moment as compressive in-plane strains were increased.

We also observe strong magnetic anisotropy in SRO

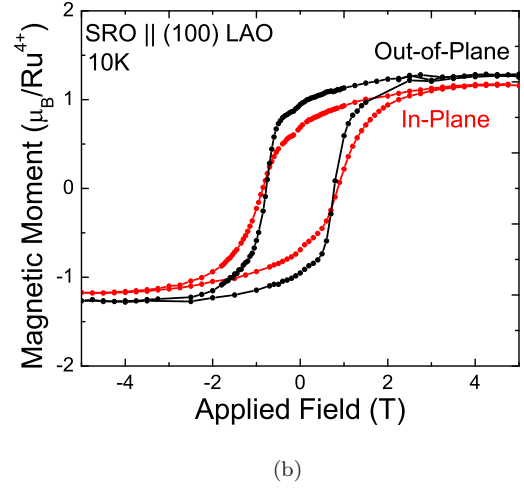
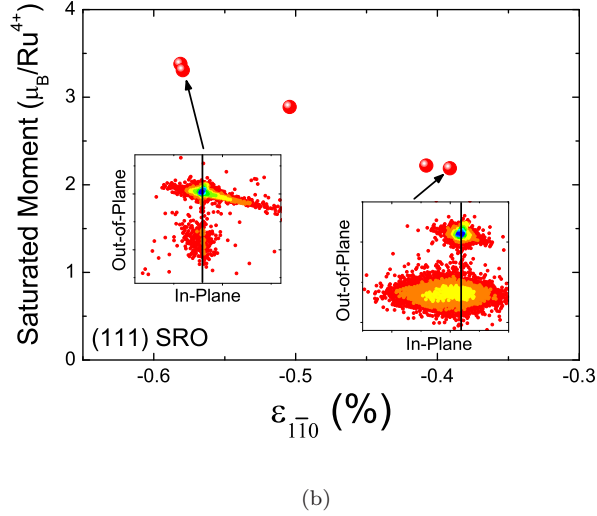
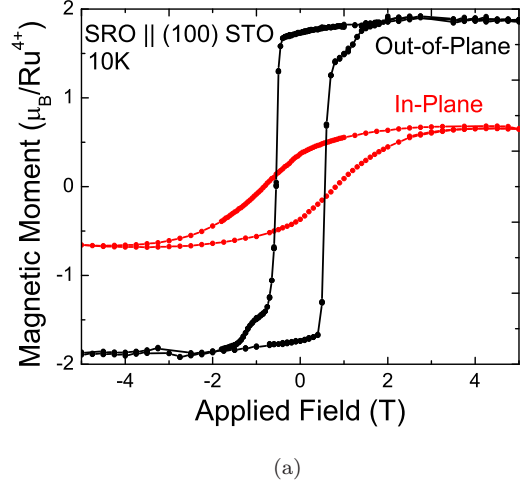
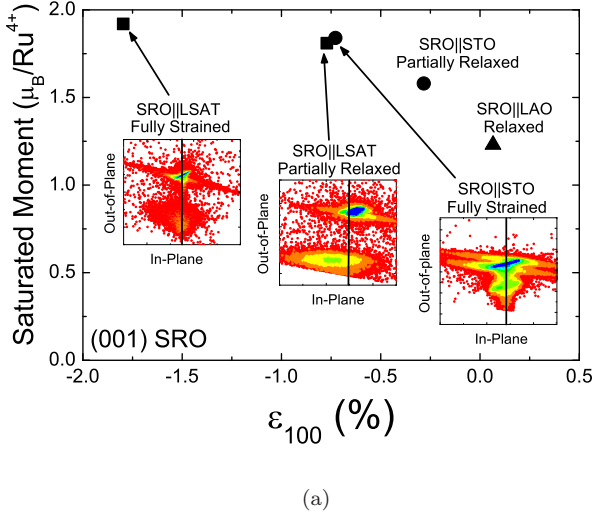


FIG. 2: Saturated magnetic moment vs. strain for films on a) (100) oriented STO, LSAT, and LAO b) (111) oriented STO. Thicknesses range from 20-120 nm. Strain values extracted from the 301 and 312 reflections, respectively show that as compressive in-plane strain increases, (100) oriented films approach a saturated magnetic moment of  $2 \mu_B/\text{Ru}^{4+}$  while (111) oriented films approach a saturated moment of  $4 \mu_B/\text{Ru}^{4+}$ . The insets are reciprocal lattice maps of several films which further demonstrate that it is the lattice distortion that determines the magnetic state.

films with a easy axis out of the plane of the film for all strained samples. The magnetic anisotropy of SRO is known to be relatively complex, with some reports showing an out-of-plane easy axis (normal to the substrate)<sup>23</sup> and others showing the easy axis at a temperature dependent angle to the film normal<sup>24</sup>. However, our observations agree with and expand upon the recent reports that for SRO films grown on both (100) and (110) STO the magnetic easy axis is out-of-plane.<sup>14,18</sup> A comparison

FIG. 3: (color online) Magnetic moment vs. Applied field at 10K with external field in the in-plane and out-of-plane direction for a) coherently strained SRO on (100) STO and b) relaxed SRO on (100) LAO.

of our in-plane (IP) and out-of-plane (OOP) hysteresis loops shows this to be the case for films in (100), (110), and (111) orientations on multiple substrate materials. Although we have not attempted to resolve the angular dependence in detail, the much higher remnant magnetization found in the OOP direction is indicative of an easy axis. Figure 3(a) and (b) show hysteresis loops taken with  $H$  in-plane and  $H$  out-of-plane for SRO on (100) STO and (100) LAO, respectively. The film on STO is coherently strained while the film on LAO has relaxed to nearly bulk lattice parameters. Although both exhibit anisotropy, the shape of the in-plane and out-of-plane loops are very different in the strained films but very similar in the relaxed LAO film. Additionally, the difference between in-plane and out-of-plane saturated mo-



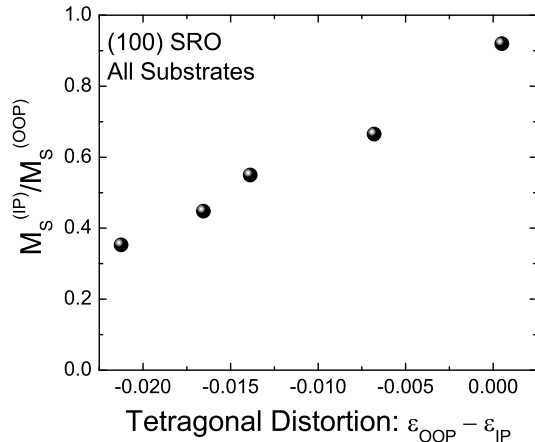


FIG. 4: Anisotropy vs. tetragonal distortion of SRO films grown on (100) STO, LSAT, and LAO at a variety of thicknesses between 20-120nm. Tetragonal distortion was calculated using reciprocal lattice maps, and anisotropy was measured by taking the ratio of film moments in a 5T field applied in-plane and out-of-plane. Anisotropy can be seen to increase with tetragonal distortion.

ments is much smaller in the relaxed film. When (100) oriented films are compared using strains calculated from reciprocal lattice maps, more heavily strained films are always more anisotropic. Figure 4 shows a more direct comparison of the tetragonal distortion and the degree of anisotropy, represented by the ratio of magnetic moments with a 5 T field applied in-plane (IP) and out-of-plane (OOP). Again assuming the strain state is well represented by the peak of the measured reciprocal lattice point, we calculate the tetragonal distortion to be  $\epsilon_{OOP} - \epsilon_{IP}$ . We can see that the magnitude of the tetragonal distortion strongly correlates with the anisotropy, further corroborating the importance of strain in magnetic anisotropy.

X-ray absorption (XA) measurements performed at beamline 6.3.1 and 4.0.2 of the Advanced Light Source showed the samples to be free of magnetic impurities such as Fe, Ni, and Co to within the sensitivity of the measurements and confirmed that the magnetism originates primarily on the  $\text{Ru}^{4+}$ , with a smaller contribution from  $\text{O}^{2-}$  ions. Typical examples of Ru and O XA spectra can be seen in Figure 5. As there is no other known example of high-spin Ru, it is not known what the XA spectra of high spin Ru should look like. However, the spectra are consistent with previously reported examples of  $\text{Ru}^{4+}$  in an octahedral environment.<sup>25</sup> Also shown in Figure 5 are typical XMCD measurements taken at 75 K with an alternating  $\pm 0.5\text{T}$  applied field at normal ( $90^\circ$ ) and grazing ( $30^\circ$ ) angles to the film surface, which allow us to confirm the SQUID magnetic anisotropy measurements and probe the origins of this effect. Application of a magnetic field in grazing geometry results in significantly less dichroism from both the  $\text{O}^{2-}$  and  $\text{Ru}^{4+}$  ions

when the field is applied out-of-plane, showing greater magnetic polarization in the normal geometry. These Ru and O spectra are indicative of an out-of-plane easy axis in agreement with the SQUID magnetic anisotropy measurements. It is interesting to note that the magnetic polarization and anisotropy is present in the O spectra, rather than the Ru alone. This is likely the result of strong Ru  $4d$  - O  $2p$  hybridization. Together the XMCD and SQUID measurements indicate a strong magnetic anisotropy in strained SRO films.

Through careful application of the XMCD sum rules to the spectra, we calculate the ratio between spin and orbital moment of films in a variety of orientations and strain states. This ratio  $m_l/m_s$  was then calibrated to saturated moments measured in the SQUID to yield the estimated magnitude of the orbital moment. Measurements on strained (100), (110), and (111) oriented samples show that both the ratio  $m_l/m_s$  and the absolute value of the orbital moment are significantly larger for strained films on STO than for relaxed films on LAO. The strained films had ratios between 8-15%, corresponding to orbital moments between  $0.24$ - $0.32 \mu_B/\text{Ru}^{4+}$  while relaxed films on LAO had much lower values of  $m_l/m_s < 5\%$  and  $m_l < 0.06 \mu_B/\text{Ru}^{4+}$ . These values are consistent with the earlier estimates of the maximum attainable moment for  $\text{Ru}^{4+}$  in a low spin state for (100) and (110) SRO films and also demonstrate that the high saturated Ru moment of (111) oriented films cannot be explained by an orbital moment contribution. Finally, the increased OOP orbital moment in the compressively strained films can be expected to increase the strength of the spin-orbit coupling and potentially cause the strong universal anisotropy.

## V. TRANSPORT

In an itinerant ferromagnet where the conduction electrons are responsible for the magnetism, changes in the magnetic properties are often accompanied by changes in electron transport. Consequently, we have performed resistivity and Hall effect measurements to provide further insight into the ground state of our SRO thin films. The results show that the variation in magnitude and symmetry of the epitaxial strain has profound effects on the electronic and magnetic ground state. Resistivity ( $\rho$ ) vs. temperature measurements indicate variation of Curie temperature with epitaxial strain. In Hall effect measurements, we see significant changes in the carrier concentration, which may reflect variation in the density of states near the Fermi level.

Our resistivity values are consistent with other high quality SRO films, with typical values ranging from 190 to  $300 \Omega\text{-cm}$  at 300K.<sup>26</sup> The residual resistivity ratio, here defined as the ratio of the resistivity value at room temperature to that at 5K, was typically between 3.5-5; these values are also in good agreement with other high-quality single-crystalline thin films.<sup>26,27</sup> Relaxed films on

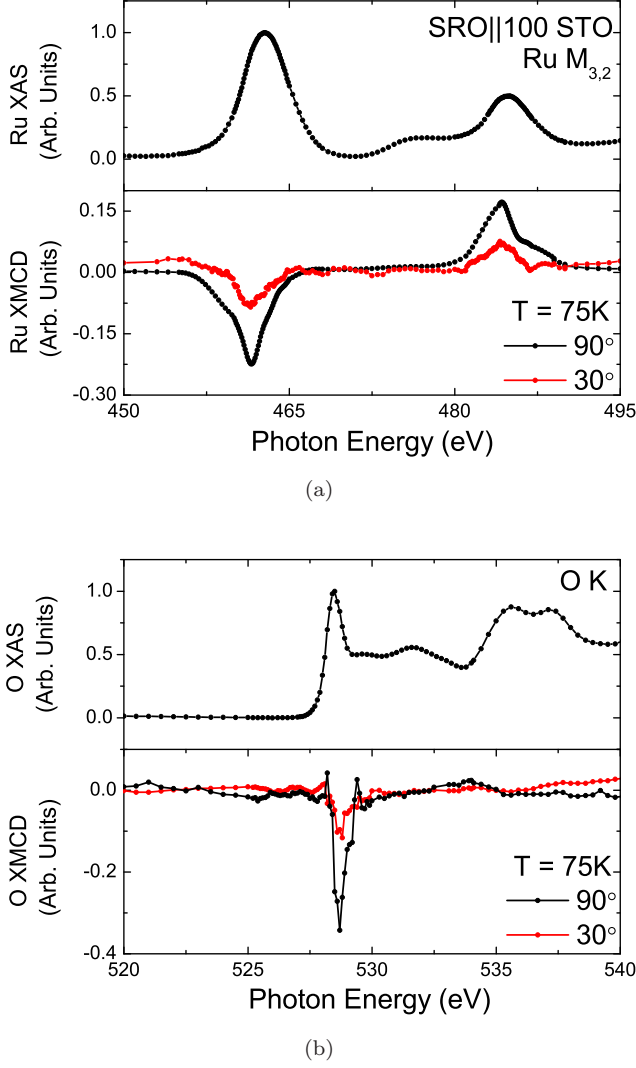


FIG. 5: (a) Ru  $M_{3,2}$  and (b) O K-edge X-ray Absorption (XA) and X-ray Magnetic Circular Dichroism (XMCD) spectra of SRO on STO. The XA spectrum is compatible with an octahedral coordination of  $Ru^{4+}$ , while the XMCD shows magnetism originating in the Ru and, to a lesser extent, the O. XMCD taken at normal ( $90^\circ$ ) and grazing ( $30^\circ$ ) incidence shows strong anisotropy in agreement with SQUID magnetometry measurements.

both (100) and (110) LAO showed the highest resistivity while films on STO and LSAT were significantly lower. In Figure 6, we see a direct comparison of films grown on all orientations of STO. SRO on (111) STO shows much higher resistivity and residual resistivity than other STO orientations. We attribute these differences to a combination of different microstructural effects and possibly changes in the effective mass due to modified band structure.

Previous studies have shown that epitaxial strain can lower the  $T_C$  of (100) oriented SRO films.<sup>22,28</sup> We corre-

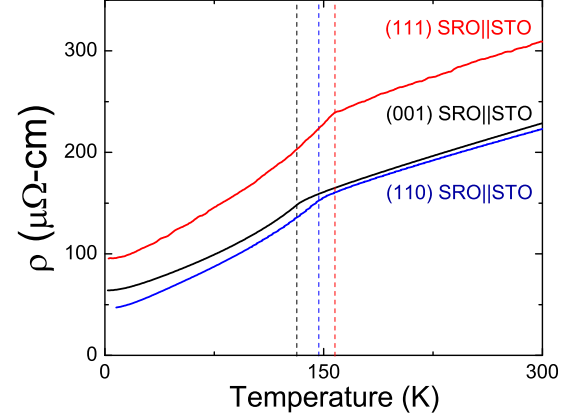


FIG. 6: (color online) Resistivity ( $\rho$ ) vs. Temperature for 65 nm thick films on (100), (110), and (111) STO showing significant variation in resistivity and transition temperature among the different orientations. The dashed lines mark the resistivity kink, and thus transition temperature, of the corresponding film.

lated the Curie temperatures ( $T_C$ ) (as determined by the peak in  $d\rho/dT$ ) with the type of distortion imposed by the substrate. Substrate orientation significantly affected  $T_C$ , with typical values of 133-137K, 142-148K and 150-154K for films on (100), (110), and (111) oriented STO, respectively. Films on LSAT and LAO followed similar trends. It is important to note that relaxed films on (100) and (110) oriented LAO were much more bulk-like than corresponding films on STO and LSAT, with transition temperatures of 150 K and 156 K respectively. Although there are a number of factors that affect the  $T_C$  of SRO thin films, including stoichiometry and strain magnitude, it is clear that the symmetry of the applied strain is an important factor in determining the strength of the magnetic exchange interaction. Thus, we can see that films in the (111) orientation have the strongest exchange interaction.

Although the Hall effect in SRO exhibits complex temperature dependent behavior, including a sign change in the vicinity of the Curie temperature,<sup>29-31</sup> we can obtain an estimate of carrier concentration from measurements in the lower temperature regime ( $<100K$ ) using a single band approximation in which  $R_{Hall} = 1/(ne)$ . In general, (111) oriented films have the highest carrier concentrations, with carrier concentrations over twice as large as (100) SRO on STO. It is at first surprising that the films with the highest resistivity also have the highest carrier concentration. However, (111) films also exhibit significantly decreased mobility which we believe to be associated with a higher incidence of defects and increased mosaic spread, as observed in residual resistivity and X-ray diffraction measurements respectively. So, the enhancement of the carrier concentration, and hence the

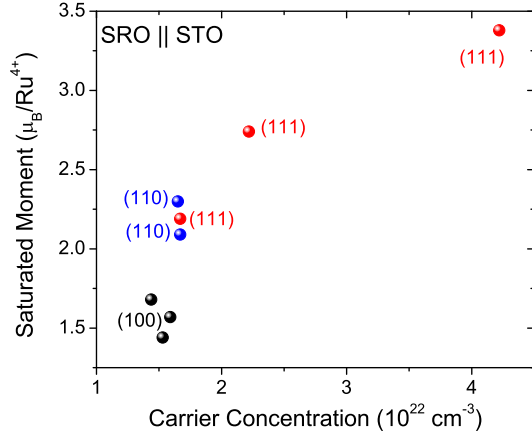


FIG. 7: Carrier concentration vs. Saturated moment at 50K for (100), (110), and (111) oriented films on STO. Across all different orientations, an increase in carrier concentration is correlated with an increase in saturated magnetic moment.

density of states at the Fermi level, can be correlated with the magnetism. Figure 7 shows the relationship between saturated Ru moments and the carrier concentrations extracted from Hall effect measurements for 30-60nm thick SRO films on STO of various orientations. Across a variety of orientations of STO with similar thickness, we find that the saturated Ru moment scales with carrier concentration, indicating an enhancement of the density of states at the Fermi level with increasing saturated moment.

## VI. DISCUSSION

Correlation of the lattice distortions, enhancement of saturated Ru moment and strong magnetic anisotropy in these SRO films lead us to conclude that it is the symmetry and magnitude of the lattice deformation that produces and controls these unusual magnetic properties. We find the degree of enhancement to be highly tunable and dependent only on the strain state. For example, a partially relaxed film on (100) LSAT whose in-plane lattice parameter is nominally 0.7% smaller than bulk. Its saturated moment is nearly identical to that of a coherently strained film on (100) STO, which is under 0.7% compressive strain (Figure 4). Both films exhibit saturated moments of  $1.8 \mu_B/\text{Ru}^{4+}$ . Alternatively, we can use the example of a fully relaxed and partially relaxed pair of films on (100) LAO which saturate at 1.3 and  $1.8 \mu_B$  per formula unit, respectively. Thus two films on different substrates with the same strain have the same saturated moment while two films on the same substrate with different strains have different saturated moments. It is clear, then, that lattice distortions play a dominant role in controlling the magnitude of the saturated mo-

ment.

The smaller saturated Ru moment found on (100) and (110) oriented films are consistent with a low-spin  $\text{Ru}^{4+}$  configuration after accounting for the orbital contribution measured with XMCD. However, moment values that greatly exceed  $2 \mu_B/\text{Ru}^{4+}$  cannot be accounted for within the low-spin  $\text{Ru}^{4+}$  local moment picture. Through X-ray diffraction and RBS, we have explicitly ruled out the possibility that the additional enhancement is due to factors such as off-stoichiometry or alternate phases. X-ray absorption measurements rule out a change in valence or the presence of magnetic impurities. Finally, XMCD demonstrates that the increase in orbital magnetic moment is much too small to explain the larger effect in (111) oriented films. Thus, we propose that the pure shear stress of the trigonal distortion imposed by the (111) substrate alters the Ru-O bonds in a way which reduces the splitting between the  $t_{2g}$  and  $e_g$  orbitals, thus enhancing the density of states at the Fermi level and effectively stabilizing a high-spin state.

This  $t_{2g}^3 e_g^1$  state would have a maximum saturated moment of  $4 \mu_B/\text{Ru}^{4+}$ . Since all of our (111) films saturate between 2 and  $4 \mu_B/\text{Ru}^{4+}$ , it is possible that the high and low-spin states coexist in thicker, partially relaxed samples where a strain gradient may be present. In fact, we see from Figure 1 that the hysteresis loops of some (111) films exhibit a "pinching" effect consistent with the coexistence of two distinct magnetic states.

Such a picture is in agreement with the demonstrated relationship between saturated magnetic moment and carrier concentration. If the  $e_g$  states are split such that the lower  $e_g$  levels become occupied, a corresponding increase in the density of states can be expected. This enhancement of the density of states should manifest itself in an increased carrier concentration, precisely as observed in our films on STO. Moreover, both the carrier concentration and saturated magnetic moment should scale with the density of states at the Fermi level. In this picture, we expect increased carrier concentration to correspond to increased saturated moment, exactly as shown in Figure 7.

We also can see conclusively from Figure 4 that the magnetic anisotropy is controlled by the magnitude of the applied lattice distortion. We can estimate the magnitude of the out-of-plane orbital magnetic moment from XMCD measurements. We find that the OOP orbital moment of compressively strained films in all orientations is enhanced relative to bulk-like relaxed films. The Bruno model of magnetocrystalline anisotropy then predicts a corresponding increase in the anisotropy energy of the compressively strained films.<sup>32,33</sup> It is therefore likely that the strong magnetic anisotropy is a direct result of enhanced OOP orbital moment in compressively strained films.

These observations provide further corroboration that all of the novel magnetic behavior can be traced back to altered bonding induced by lattice distortions. Bulk SRO is already known to have strong spin orbit coupling rela-



tive to most magnetic  $3d$  systems, likely due to the relatively heavy Ru ions.<sup>8</sup> However, there are several avenues by which this interaction might be enhanced. Distortions of the Ru-O octahedral could anisotropically reduce orbital overlap and decrease the crystal field splitting. Such a disruption of orbital overlap could reduce the quenching of the orbital moment, leading to strong anisotropy in the orbital moment.

Thus we see that the anisotropy, enhanced saturated Ru moments, and increases in carrier density are all consistent with a strain-induced stabilization of a high spin Ru state. We can now form a complete picture of the magnetic state. Compressive strain results in a distortion of the Ru-O octahedra, simultaneously weakening the OOP bonding and splitting the  $e_g$  energy levels. The weakened OOP bonding reduces the quenching of the orbital moment and results in strong uniaxial anisotropy while the altered band structure enhances the saturated moment and, in (111) oriented films, stabilizes a high-spin Ru state.

## VII. CONCLUSIONS

In conclusion, we have shown enhanced magnetization in SRO thin films which cannot be explained either by magnetic impurities or an increase in orbital moment. Rather, both magnetic and transport data are strongly

indicative of a high spin state of  $\text{Ru}^{4+}$ . We have demonstrated that the enhancement of the magnetic moment can be controlled through the application of compressive in-plane epitaxial strain. It is likely that this distortion stabilizes a high spin state through decreased orbital overlap and a corresponding enhancement in the density of states at the Fermi level by the newly split  $e_g$  band. In all cases, the decrease in orbital overlap results in the enhancement of the saturated magnetic moment and universal anisotropy direction even in SRO films of different orientations. This universal anisotropy direction is manifested as an out-of-plane easy axis in all compressively strained films of (100), (110), and (111) orientation and is likely due to the enhancement of the out-of-plane orbital magnetic moment. Finally, we have shown that it is possible to tune the effects of this distortion by varying the orientation and magnitude of this strain, particularly in the case of (111) oriented films which exhibit evidence of a high spin  $\text{Ru}^{4+}$  and the coexistence of two spin states.

We would like to thank J. Rondinelli and N. Spaldin for fruitful discussions, and K. M. Yu for his assistance in RBS data collection. This work and the Advanced Light Source are supported by the Director, Office of Science, Office of Basic Energy Sciences, of the U.S. Department of Energy under Contract No. DE-AC02-05CH11231. F. J. W. is supported by the Army Research Office under Grant No. MURI W911NF-08-1-0317.

- 
- <sup>1</sup> Y. Moritomo, H. Kuwahara, and Y. Tokura, *Physica B* **237-238**, 26 (1997)
  - <sup>2</sup> R. S. Liu, C. H. Shen, and S. F. Hu, *Int. J. Inorg. Mater.* **3**, 1063 (2001)
  - <sup>3</sup> Y. Suzuki, H. Y. Hwang, S-W. Cheong, and R.B. van Dover, *Appl. Phys. Lett.* **71**, 140 (1997)
  - <sup>4</sup> D. J. Singh, *J. Appl. Phys.* **79**, 4818 (1996)
  - <sup>5</sup> N. Hiraoka, M. Itou, A. Deb, Y. Sakurai, Y. Kakutani, A. Koizumi, N. Sakai, S. Uzuhaara, S. Miyaki, H. Koizumi, K. Makoshi, N. Kikugawa and Y. Maeno, *Phys. Rev. B* **70**, 054420 (2004)
  - <sup>6</sup> K. Maiti, *Phys. Rev. B* **73**, 235110 (2006)
  - <sup>7</sup> P. B. Allen, H. Berger, O. Chauvet, L. Forro, T. Jarlborg, A. Junod, B. Revaz, and G. Santi, *Phys. Rev. B* **53**, 4393 (1996)
  - <sup>8</sup> M. C. Langer, Ph.D. Thesis, University of California, Berkeley (2009)
  - <sup>9</sup> S. N. Bushmeleva, V. Yu. Pomjakushin, E. V. Pomjakushina, D. V. Sheptyakov, and A. M. Balagurov, *J. Magn. Magn. Mater.* **305**, 491 (2006)
  - <sup>10</sup> A. Kanbayasi, *J. Phys. Soc. Jpn.* **41**, 1876 (1976)
  - <sup>11</sup> P. S. Anil Kumar, P. A. Joy, and S. K. Date, *Physica B* **269**, 356 (1999)
  - <sup>12</sup> D. Toyota, I. Ohkubo, H. Kumigashira, M. Oshima, T. Ohnishi, M. Lippmaa, M. Takizawa, A. Fujimori, K. Ono, M. Kawasaki, and H. Koinuma, *Appl. Phys. Letters* **87**, 162508 (2008)
  - <sup>13</sup> P. Mahadevan, F. Aryasetiawan, A. Janotti, and T. Sasaki, *arXiv:0812.2098v2* (2009)
  - <sup>14</sup> R. Palai, H. Huhtinen, J. F. Scott, and R. S. Katiyar, *Phys. Rev B* **79**, 104413 (2009)
  - <sup>15</sup> A. Grutter, F. Wong, E. Arenholz, M. Liberati, A. Vailionis, and Y. Suzuki, *Appl. Phys. Lett.* **96**, 082509 (2010)
  - <sup>16</sup> A. Grutter, F. Wong, E. Arenholz, M. Liberati, and Y. Suzuki, *J. Appl. Phys.* **107**, 09E138 (2010)
  - <sup>17</sup> M. Bohra, C. P. Wu, H. J. Yeh, Y. H. Cheng, C. C. Peng, and H. Chou, *J. Appl. Phys.* **109**, 07D728 (2011)
  - <sup>18</sup> X. W. Wang, Y. Q. Zhang, H. Meng, Z. J. Wang, D. Li, and Z. D. Zhang, *J. Appl. Phys.* **109**, 07D707 (2011)
  - <sup>19</sup> A. T. Zayak, X. Huang, J. B. Neaton, and K. M. Rabe, *Phys. Rev. B* **77**, 214410 (2008)
  - <sup>20</sup> C. W. Jones, P. D. Battle, P. Lightfoot, and W. T. A. Harrison, *Acta Cryst.* **C45**, 365 (1988)
  - <sup>21</sup> C. B. Eom, R. J. Cava, R. M. Fleming, J. M. Phillips, R. B. van Dover, J. H. Marshall, J. W. P. Hsu, J. J. Krajewski, and W. F. Peck Jr., *Science* **258**, 1766 (1992)
  - <sup>22</sup> Q. Gan, R. A. Rao, C. B. Eom, J. L. Garrett, and M. Lee, *Appl. Phys. Letters* **72**, 978 (1998)
  - <sup>23</sup> L. Klein, J. S. Dodge, T. H. Geballe, A. Kapitulnik, A. F. Marshall, L. Antognazza and K. Char, *Appl. Phys. Lett.* **66**, 2427 (1995)
  - <sup>24</sup> M. Ziese, I. Vrejoiu, and D. Hesse, *Phys. Rev. B* **81**, 184418 (2010)
  - <sup>25</sup> J. Okamoto, T. Okane, Y. Saitoh, K. Terai, S.-I. Fujimori, Y. Muramatsu, K. Yoshii, K. Mamiya, T. Koide, A. Fujimori, Z. Fang, Y. Takeda, and M. Takano, *Phys. Rev. B* **76**, 184441 (2007)
  - <sup>26</sup> Q. X. Jia, F. Chu, C. D. Adams, X. D. Wu, M. Hawley, J.

- H. Cho, A. T. Findikoglu, S. R. Foltyn, J. L. Smith, and T. E. Mitchell, *J. Mater. Res.* **11**, 2263 (1996)
- <sup>27</sup> W. Siemons, G. Koster, A. Vailionis, H. Yamamoto, D. H. A. Blank, and M. R. Beasley *Phys. Rev. B* **76**, 075126 (2007)
- <sup>28</sup> Y. J. Chang, J. I. Kim, and C. U. Jung, *J. of Magnetism* **13**, 61 (2008)
- <sup>29</sup> S. C. Gausepohl, Mark Lee, R. A. Rao and C. B. Eom, *Phys. Rev. B* **54**, 8996 (1996)
- <sup>30</sup> Yevgeny Kats, Isaschar Genish, Lior Klein, James W. Reiner, and M. R. Beasley, *Phys. Rev. B* **70**, 180407 (2004)
- <sup>31</sup> M.-H. Kim, G. Acbas, M.-H. Yang, M. Eginligil, P. Khali-fah, I. Ohkubo, H. Christen, D. Mandrus, Z. Fang, and J. Cerne, *Phys. Rev. B* **81**, 235218 (2010)
- <sup>32</sup> P. Bruno, *Phys. Rev. B* **39**, 865 (1989)
- <sup>33</sup> G. van der Laan, *J. Phys. Condens. Matter* **10**, 3239 (1998)